Supplementary information for: Symmetry-informed design of magnetoelectric coupling in the new manganite perovskite CeBaMn$_2$O$_6$
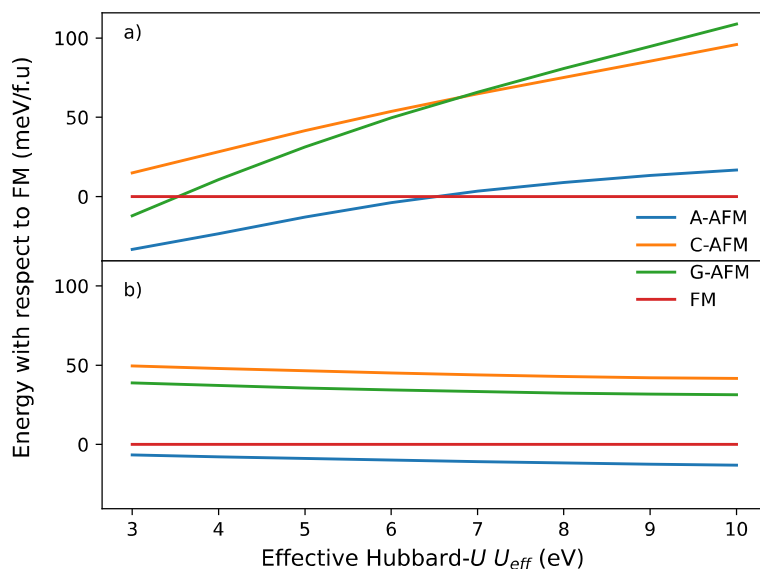

Fig S1 : The effect of a variation of Hubbard-U on the relative stabilities of various spin orderings. a) Variation of U on the Mn $3d$ electrons causes a transition to a stable FM state above 6eV. b) Variation of U on the Ce $4f$ electrons does not affect the relative stabilities of the spin orderings . Ce^{4+} has an empty f shell and is therefore expected to play a negligible role in the magnetic properties of CeBaMn$_2$O$_6$.
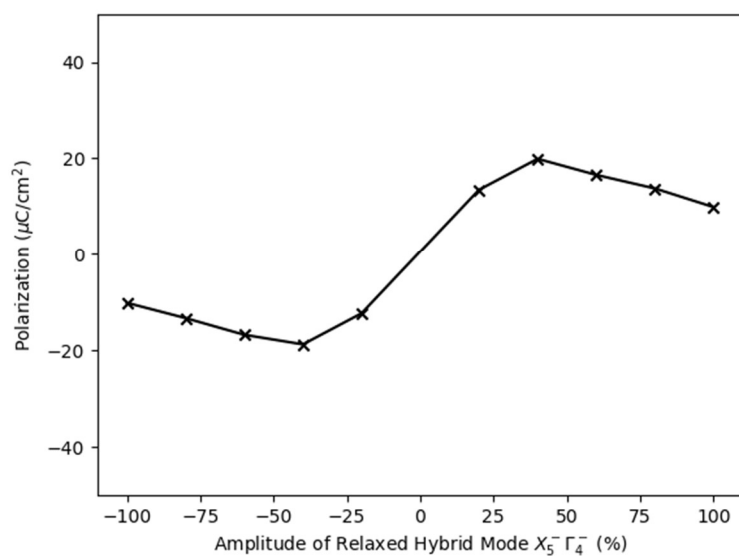

Fig S2 : Polarization as a function of amplitude of the hybrid $X_5^- \Gamma_4^-$ mode involved in our proposed switching scheme. The fully relaxed polar domains have electric polarisations of $\pm 9.90 \mu C/cm^2$.
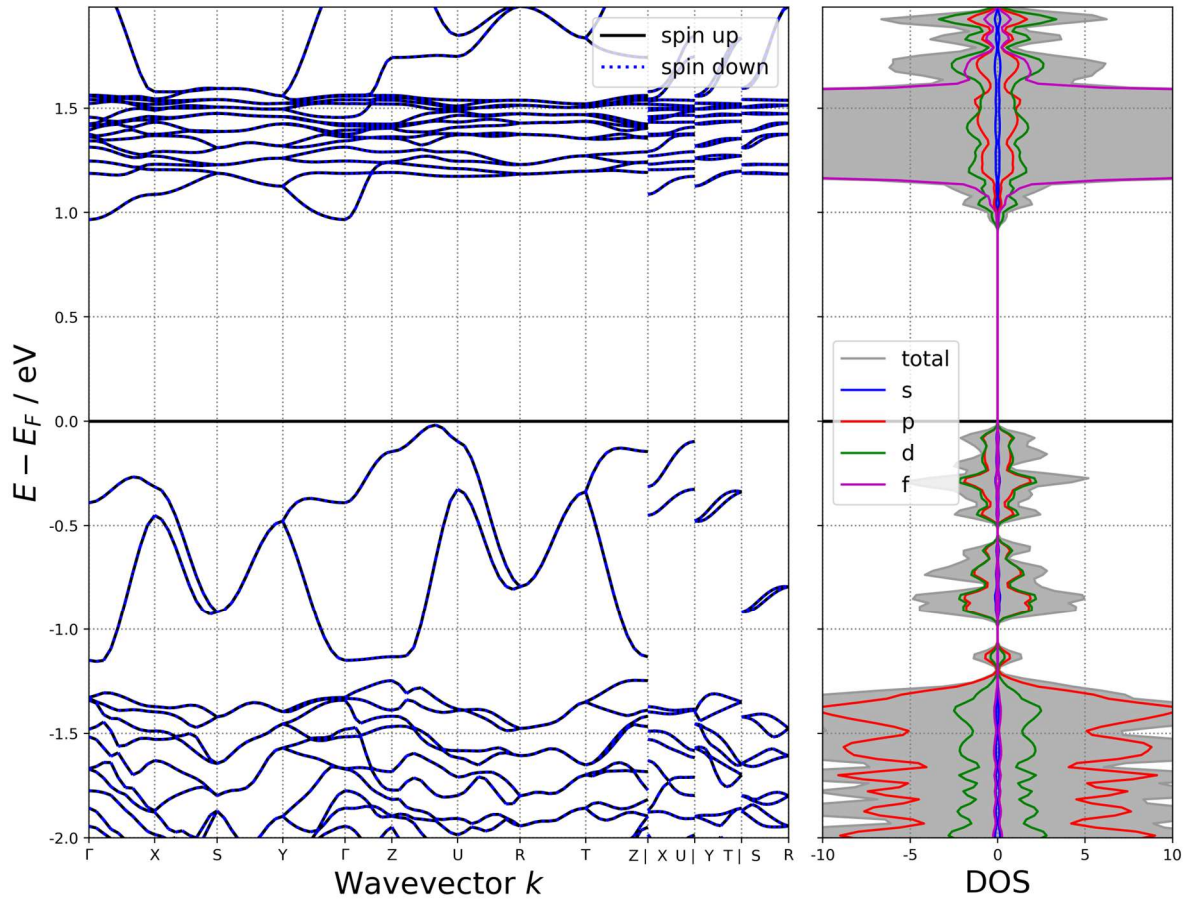
Fig S3 : Electronic structure of A-site layered, A-type CeBaMn2O6. a) Bandstructure indicating an indirect optical band gap of 0.98eV. b) Transition occurs between valence band states of predominantly hybridised Mn-*d* and O-*p* character to conduction band states of predominantly Mn-*d* character. Calculated with $U_{Mn-d} = 5\ eV, J_{Mn-d} = 1.5\ eV, U_{Ce-f} = 10\ eV, J_{Ce-f} = 0eV$

Table S1: Comparison of irrep amplitudes between experimentally determined LaMnO$_3$ [1] structural modes, a relaxed LaMnO$_3$ cell obtained in the present investigation and the A-site layered CeBaMn$_2$O$_6$ structure. The largest difference in the distortions between the two structures comes from the antiphase R_5^- octahedral tilts. This could be due to the slight increase in ionic radius in going from La to Ce/Ba and thus increasing the tolerance factor closer to the cubic ideal. The irrep amplitudes (Q) have been normalised with respect to the parent $Pm\bar{3}m$ structure (parameter A_p in ISODISTORT).

Property	LaMnO$_3$ Exp (Å)	LaMnO$_3$ DFT (Å)	CeBaMn$_2$O$_6$ – DFT (Å)
a	5.7461	5.7987	5.8182
b	7.6637	7.6095	7.7379
c	5.5332	5.5051	5.5225
$Q(\Gamma_4^-)$	N/A	N/A	0.51738
$Q(R_4^-)$	0.11192	0.11669	0.08061
$Q(R_5^-)$	1.27440	1.31399	0.97528
$Q(X_1^+)$	N/A	N/A	0.69660
$Q(X_5^-)$	0.60501	0.68325	0.59203
$Q(M_2^+)$	0.97072	1.01568	1.01077
$Q(M_3^+)$	0.35299	0.37726	0.35831
$Q(M_5^-)$	N/A	N/A	0.33762

Table S2: Magnetocrystalline anisotropy energy and magnetic moments of various easy axes in A-type *A*-site layered $CeBaMn_2O_6$. Obtained non-self-consistently by freezing the charge density of the collinear self-consistent calculation and then rotating the easy axis. The quantisation axes and magnetic moments are listed with respect to the *Pnma* setting of the $LaMnO_3$ structure.

Quantisation Axis Direction	Ground State Energy (meV/f.u.)	Magnetic Moment (μ_B/Mn)
[001]	1.4	(0,0,0)
[100]	0.0	(0, 0.0289,0)
[010]	1.9	(0.0008,0,0)
[101]	0.7	(0,0,0.0042)
[011]	1.5	(0.0003,0,0.0042)
[110]	1.0	(0.0002, 0.0002, 0.0026)
[111]	1.4	(0,0,0)

Table S3. Lattice parameters, atomic coordinates, and refinements statistics obtained from Rietveld fits against synchrotron XRD data collected at I11, Diamond Light Source (λ = 0.8240 Å) for $CeBaMn_2O_6$ at 300 K.

Space group	$Pm\bar{3}m$				
a (Å)	3.916865(2)				
b (Å)	3.916865(2)				
c (Å)	3.916865(2)				
α (°)	90				
β (°)	90				
γ (°)	90				
R_p (%)	1.85				
R_{wp} (%)	3.42				
Site	x	y	z	Occupancy	U_{iso} (Å²)
Ce	0	0	0	0.5	0.00426(3)
Ba	0	0	0	0.5	0.00426(3)
Mn	0.5	0.5	0.5	1	0.00142(4)
O	0.5	0.5	0.5	1	0.0294(2)

Table S4. Lattice parameters, atomic coordinates, and refinements statistics obtained from Rietveld fits against NPD data collected on WISH for $CeBaMn_2O_6$ at 300 K.

Space group	$Pm\bar{3}m$				
a (Å)	3.91520(7)				
b (Å)	3.91520(7)				
c (Å)	3.91520(7)				
α (°)	90				
β (°)	90				
γ (°)	90				
R_p (%)	4.95				
R_{wp} (%)	7.39				
Site	x	y	z	Occupancy	U_{iso} (Å^2)
Ce	0	0	0	0.5	0.023(1)
Ba	0	0	0	0.5	0.023(1)
Mn	0.5	0.5	0.5	1	0.0166(1)
O	0.5	0.5	0.5	1	[1]

[1] Anisotropic displacement parameters (ADPs) were refined for the oxygen site, yielding $U_{11} = 0.020(2)$ Å^2, $U_{22} = U_{33} = 0.079(1)$ Å^2, $U_{12} = U_{13} = U_{23} = 0$.

Table S5. Lattice parameters, atomic coordinates, and refinement statistics obtained from Rietveld fits against NPD data collected on WISH for $CeBaMn_2O_6$ at 1.5 K.

Space group	$Pm\bar{3}m$				
a (Å)	3.90966(7)				
b (Å)	3.90966(7)				
c (Å)	3.90966(7)				
α (°)	90				
β (°)	90				
γ (°)	90				
R_p (%)	6.08				
R_{wp} (%)	8.07				
Site	x	y	z	Occupancy	B_{iso} (Å^2)
Ce	0	0	0	0.5	0.024(1)
Ba	0	0	0	0.5	0.024(1)
Mn	0.5	0.5	0.5	1	0.018(1)
O	0.5	0.5	0.5	1	[1]

[1] Anisotropic displacement parameters (ADPs) were refined for the oxygen site, yielding $U_{11} = 0.018(1)$ Å^2, $U_{22} = U_{33} = 0.078(1)$ Å^2, $U_{12} = U_{13} = U_{23} = 0$.

Table S6. Reflection conditions for mixed-tilt systems based on the zone axis diffraction patterns collected for CeBaMn$_2$O$_6$ (adapted from Supplementary Reference 2). 'e' and 'o' correspond to even and odd *hkl* indices, respectively. Conditions highlighted in bold correspond to sets of reflections which are observed in CeBaMn$_2$O$_6$. Note that here the reflection conditions for the *Pnma* tilt system $a^-b^+a^-$ have been listed with respect to the non-standard *Pbnm* setting ($a^-a^-c^+$) to facilitate comparison to the other possible tilt systems.

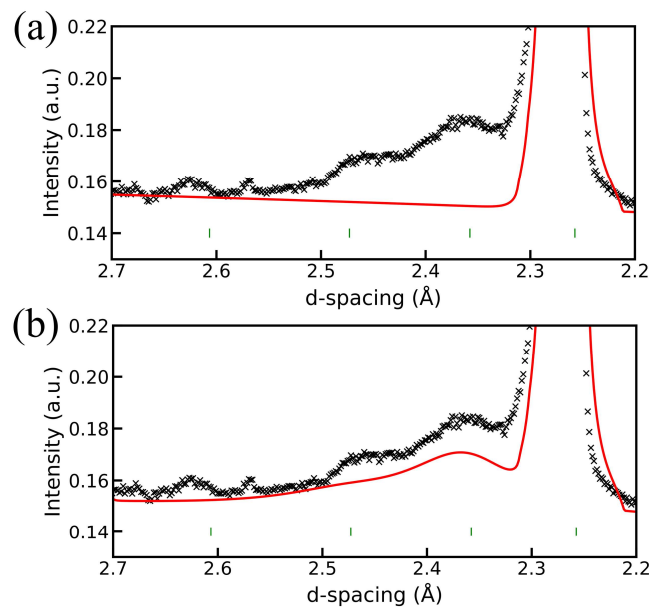| Zone axis	$a^0b^-c^+$	$a^-b^-c^+$	$a^+a^+c^-$	$a^-a^-c^+$
[001]	**½(ooe)**	**½(ooe)**	**½(ooe)**	**½(ooe)**
[110]	½(ooo) + ½(ooe) + ½(eeo)	½(ooo) + ½(ooe) + ½(eeo)	½(ooe)	**½(eeo)**
<111>	**½(ooe)**	**½(ooe)**	**½(ooe)**	**½(ooe)**
Observed?	N	N	N	**Y**

Figure S4. Excerpts of Rietveld fits against NPD data collected on the backscattering bank at 1.5 K using (a) the untilted $Pm\bar{3}m$ model (as shown in Figure 3b in the main text) and (b) the *hkl*-dependent size-broadened *Pnma* model described in the main text.
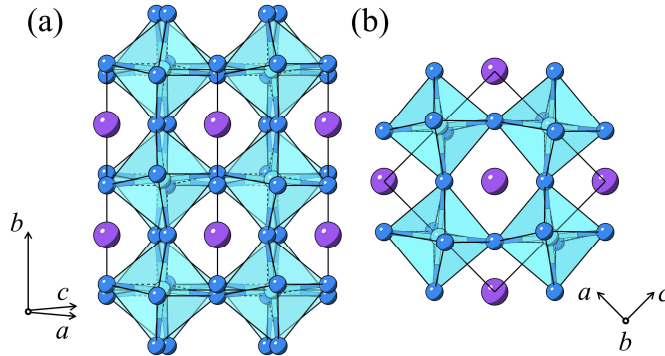
Figure S5. Final refined *Pnma*-type model of CeBaMn$_2$O$_6$. The octahedral tilt angles are 5.85° and 5.08° for (a) the R$_5^-$ ($a^-b^0a^-$) and (b) M$_2^+$ ($a^0b^+a^0$) tilt modes, respectively.

Table S7. Selected parameters obtained from the Rietveld fits using the *Pnma*-like model, including the size of symmetry-lowered domains extracted from the Scherrer-type broadening term (Eq. 3 in the main text) in the refinements. Equivalent parameters obtained for the Rietveld-refined untilted *Pm$\bar{3}$m* model as well as our relaxed DFT structure (Table S1) are provided for reference. Mode amplitudes (Q) have been normalised with respect to the parent *Pm$\bar{3}$m* cell (parameter A_p in ISODISTORT). A single isotropic ADP was refined for the oxygen sites to ensure comparability between the two structural models.

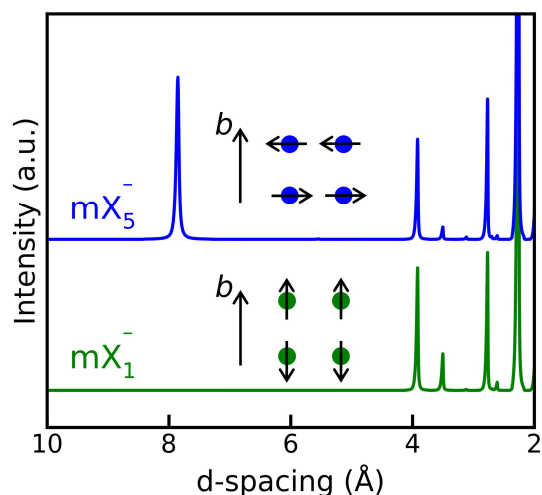|	*Pnma* model	*Pm$\bar{3}$m* model	Relaxed DFT structure
Size (nm)	4.3(3)	0	–
$Q(\mathrm{M}_2^+)$ (Å)	0.36(2)	0	1.01077
$Q(\mathrm{R}_5^-)$ (Å)	0.58(1)	0	0.97528
O U_iso (Å^2)	0.006(1)	0.029(1)	–
R_p (%)	3.92	4.74	–
R_wp (%)	5.19	6.35	–

Figure S6. Simulated diffraction patterns for the two possible A-type AFM orderings in $CeBaMn_2O_6$. Representative magnetic structures are depicted for each pattern.
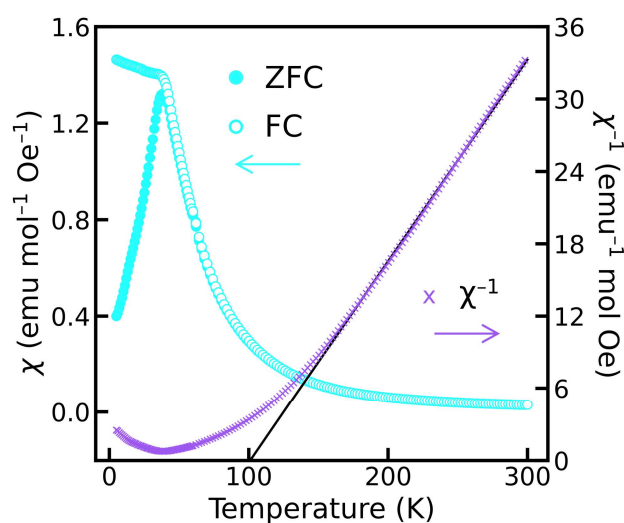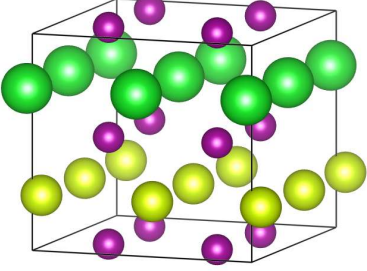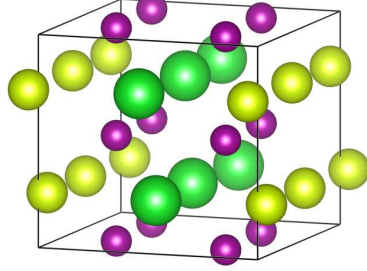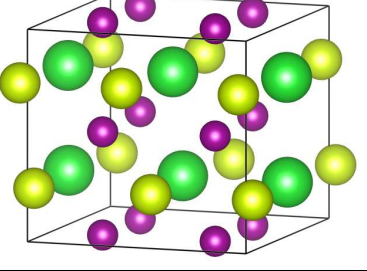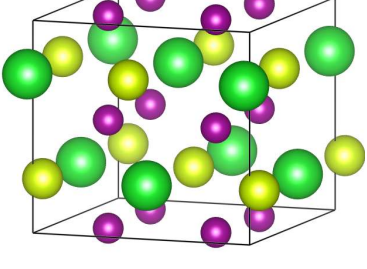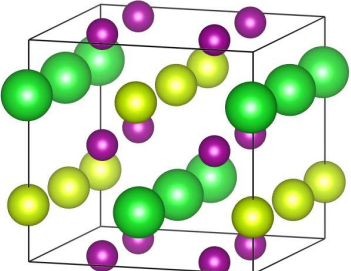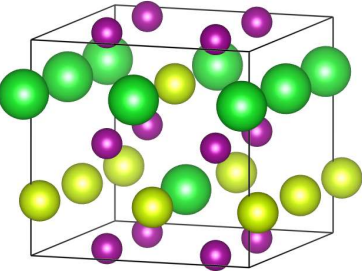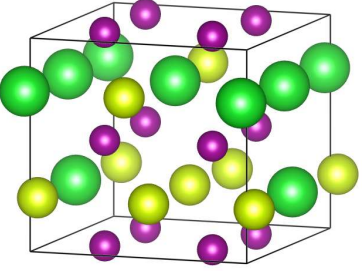

Figure S7. Zero-field-cooled (ZFC) and field-cooled (FC) magnetic susceptibility (χ) data collected between 4 and 300 K in an applied field of 500 Oe. The solid black line depicts the fit of a Curie-Weiss expression against the inverse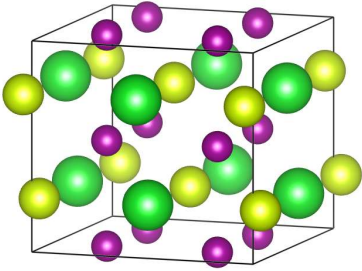 susceptibility (χ^{-1}) above 150 K; $C = 5.96(1)$ emu K^{-1} mol^{-1}, $\theta = 101(1)$ K. The Curie constant corresponds to an effective moment of 4.89 μ_B, which is in excellent agreement with the expected spin-only value for Mn^{3+} ($\sim$4.90 μ_B).

Table S8: Alternative cation schemes. Each cation layered was added to the relaxed CeBaMn$_2$O$_6$ structure and then allowed to fully relax under a structural relaxation. The *k*-point labels of all structural distortions are included here – all cation orderings considered have distortions that transforming as irreducible representations of the same *k*-points. This makes the alternative structures difficult to identify with diffraction techniques.

Cation Ordering	Space Group	Energy (meV/f.u)	*k*-Points of all structural irreps	Cation Ordering Irrep and Direction
[010] Layer	*Pmc2$_1$*	119.7	GM,X,M,R	$X_1^+(0; a; 0)$
[100] Layer	*P2$_1$/m*	0.0	GM,X,M,R	$X_1^+(0; a; b)$
[001] Layer	*Pm*	0.0	GM,X,M,R	$X_1^+(a; b; c)$
Rocksalt	*Pm*	314.0	GM,X,M,R	$R_1^+(a)$

Columnar	$P2_1/m$	77.4	GM,X,M,R	$M_1^+(0;a;0)$
Alternative Columnar	Pm	219.7	GM,X,M,R	$M_1^+(a;b;c)$ $R_1^+(a)$ $X_1^+(a;b;c)$
Single Substitution	Pm	277.4	GM,X,M,R	$M_1^+(a;b;c)$ $R_1^+(a)$ $X_1^+(a;b;c)$
Double Substitution	Pm	107.0	GM,X,M,R	$R_1^+(a)$ $X_1^+(a;b;c)$

Supplementary Note 1. Further symmetry details of the proposed magnetoelectric coupling scheme.

As stated in the main text, our proposed magnetoelectric scheme relies on the presence of a combination of structural and magnetic symmetry-breakings which couple to form invariant terms in a Landau-like free energy expansion about the high-symmetry structure. Provided crystal momentum, parity, and time reversal symmetry are preserved, the invariant terms take the following form:

$$P\,\xi_1\xi_2 \tag{1}$$

$$M\,\xi_1\xi_3. \tag{2}$$

Here, we limit our analysis of the invariant terms to order parameters which appear coupled linearly at the third order, thus we only consider terms which can always adopt a sign so as to lower the free energy of the system. Accordingly, we assume the order parameter directions (OPDs) of the irreps which describe the transformation of these order parameters with respect to the aristotype symmetry take special directions, thus simplifying any resulting coupling terms. We note that, in this example, ξ_n ($n = 1, 2, 3$) represent the transformations of different irreps. The irreps in Eq. (1) are therefore restricted to transform such that: ξ_1 and ξ_2 must have equal crystal momentum, and they must be of opposite parity with respect to inversion symmetry (given that the polarization component represented by P is inversion-odd, hence allowing Eq.(1) to be inversion-even overall); and the irreps in Eq. (2) are restricted to transform such that ξ_1 and ξ_3 have equal crystal momentum, they must be of opposite parity with respect to inversion, and they must be time-odd (given the ferromagnetic component represented by M is also time-odd, allowing Eq.(2) to obey time-reversal symmetry).

In the specific case of the CeBaMn$_2$O$_6$ system, the full set of desired order parameters transforms with respect to the $Pm\bar{3}m$ aristotype structure as $X_1^+ \oplus X_5^- \oplus mX_5^-$ and an OPD of OP(0;a;0|0,0;b,b;0,0|0,0;c,c;0,0). Here, we use the notation used in ISODISTORT [3] where the vertical bars ('|') denote divisions between the different irreps and the semi-colons denote divisions between different OPDs due to the degeneracy of the k-vector in the aristotype structure. The invariant term in Eq. (1) then becomes $\Gamma_4^- X_5^- X_1^+$, while the invariant term in Eq. (2) becomes $m\Gamma_4^+ X_5^- mX_5^-$. Note that, at least in practice, the X_5^- antipolar cation displacements are produced via the action of a separate trilinear coupling term of the form $M_2^+ R_5^- X_5^-$, where the corresponding OPD for the order parameter is specified as OP(0;0;a|b,0,b|0,0;c,c;0,0), so the predicted $Pmc2_1$ symmetry of the desired magnetoelectric phase is only obtained through careful propagation of the OPDs associated with both $X_1^+ X_5^- mX_5^-$ and $M_2^+ R_5^- X_5^-$ invariant terms.

Supplementary Note 2. Substantiating the nominal Ce^{4+} and Mn^{3+} oxidation states.

The application of our magnetoelectric coupling scheme to $CeBaMn_2O_6$ is based on the nominal oxidation states of Ce and Mn being +4 and +3, respectively. To corroborate these nominal oxidation states in our as-synthesized samples, we performed both physical and magnetic property measurements as described in the main text. DC resistivity measurements (Figure S8) reveal that $CeBaMn_2O_6$ adopts the same insulating ground state as $LaMnO_3$. This is in contrast to analogous $LnBaMn_2O_6$ ($Ln = Pr^{3+}$, Nd^{3+}) manganites, wherein a characteristic metal-insulator transition is observed upon cooling [4,5]. This metal-insulator transition reflects the presence of the double exchange interaction between Mn^{3+} and Mn^{4+} centers; the lack of any analogous metal-insulator transition in $CeBaMn_2O_6$ refutes the possibility of any significant mixed valency on the Mn site, demonstrating the nominal Ce^{4+} and Mn^{3+} oxidation state assignments to be valid. Additionally, spin-freezing transitions have only been observed in $LnBaMn_2O_6$ manganites for $r_A < 1.27$ Å ($Ln = Y^{3+}$, Dy^{3+}–Sm^{3+}), while ferromagnetic or magnetically inhomogeneous ground states are typically observed for larger Ln^{3+} cations [4-7]. The spin-freezing transition we observe in $CeBaMn_2O_6$ (Figure S7) clearly supports the nominal Ce^{4+} valence ($r_A = 1.14$ Å) rather than Ce^{3+} ($r_A = 1.34$ Å).
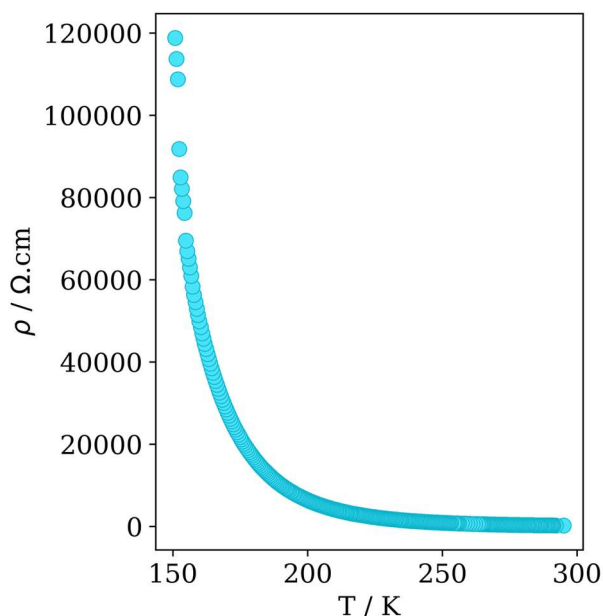

Figure S8. DC resistivity data below 300 K, showing that the sample is semiconducting before eventually becoming too resistive to measure. No metal-insulator transitions are observed in this temperature range (as otherwise seen in $Pr^{3+}BaMn^{3.5+}_2O_6$ and $Nd^{3+}BaMn^{3.5+}_2O_6$), substantiating the lack of any significant double exchange interaction and evidencing the nominal Ce^{4+}/Mn^{3+} oxidation states.

Supplementary references

1 Wollan, E. O.; Koehler, W. C. Neutron Diffraction Study of the Magnetic Properties of the Series of Perovskite-Type Compounds [(1-x)La,xCa]MnO$_3$. *Phys. Rev.* **1955**, *100*, 545.

2 Woodward, D.I.; Reaney, I. M. Electron diffraction of tilted perovskites. *Acta Cryst.* **2005**, B*61*, 387–399.

3 Campbell, B. J.; Stokes, H. T.; Tanner, D. E.; Hatch, D. M. ISODISPLACE: A Web-Based Tool for Exploring Structural Distortions. *J. Appl. Crystallogr.* **2006**, *39*, 607–614.

4 Trukhanov, S. V.; Troyanchuk, I. O.; Hervieu, M.; Szymczak, H.; Bärner, K. Magnetic and Electrical Properties of LBaMn$_2$O$_{6-\gamma}$ (L=Pr, Nd, Sm, Eu, Gd, Tb) Manganites. *Phys. Rev. B* **2002**, *66*, 184424.

5 Akahoshi, D.; Uchida, M.; Tomioka, Y.; Arima, T.; Matsui, Y.; Tokura, Y. Random Potential Effect near the Bicritical Region in Perovskite Manganites as Revealed by Comparison with the Ordered Perovskite Analogs. *Phys. Rev. Lett*. **2003**, *90*, 177203.

6 Nakajima, T.; Yoshizawa, H.; Ueda, Y. A-Site Randomness Effect on Structural and Physical Properties of Ba-Based Perovskite Manganites. *J. Phys. Soc. Jpn.* **2004**, *73*, 2283–2291.

7 Subías, G.; Blasco, J.; Cuartero, V.; Lafuerza, S.; Simonelli, L.; Gorni, G.; Castro, M.; García, J. Effects of A -Site Ordering on the Mn Local Structure and Polar Phases of RBaMn2O6 (R = La, Nd, Sm, and Y). *Phys. Rev. B* **2023**, *107*, 165133.